RESEARCH ARTICLE

Carbon nanotube hybrid nanofluid induced by a stretched sheet with aligned magnetic field

S.M. Zokri[1],*, N.H.A.M. Syaiful[1], N.S. Arifin[2], N. Zullpakkal[1] and N.A. Salahudin[1]

[1]College of Computing, Informatics and Mathematics, Universiti Teknologi MARA (UiTM) Johor Branch, Pasir Gudang Campus, 81750 Masai, Johor, Malaysia
[2]College of Computing, Informatics and Mathematics, Universiti Teknologi MARA (UiTM) Johor Branch, Segamat Campus, 85000 Segamat, Johor, Malaysia

ABSTRACT - Hybrid nanofluid are a new fluid created by combining two different types of nanoparticles dispersed in a base fluid to enhance the properties of base fluid. The incorporation of carbon nanotubes (CNTs) into a base fluid greatly enhances heat transfer performance over metal-based nanofluids. Partial differential equations (PDEs) are then transformed into simpler form of Ordinary differential equations (ODEs) using similarity transformation variables. The obtained ODEs are then encoded in Maple software using the Runge-Kutta Fehlberg Fourth Fifth (RKF45) method. By comparing the findings with those from earlier research, the authenticity of the result is confirmed. The results and discussion are focused on several parameters, including the stretching parameter, heat sink/source parameter, magnetic field parameter and aligned angle parameter over the velocity and temperature profiles. The results show that the velocity profile increases due to the increasing stretching parameter and decreases due to increasing aligned angle parameter and magnetic field parameter. The increasing value of heat source/sink parameter showed no effect on velocity. The temperature profile increases due to the increasing magnetic field parameter and aligned angle parameter. Meanwhile, the temperature profile decreases owing to the increase of stretching parameter and heat source/sink parameter. Findings of this study is related to the aerospace applications, specifically in the development of thermal protection systems where the thermal load management depends on the material conductive properties.

1. INTRODUCTION

Nanofluids are fluids containing nanoparticles that disperse into the base fluids. This nanofluids term was first proposed in 1995 by Stephen Choi to enhance the thermal performance and heat transfer capacity [1]. Since the discovery, nanofluids has enhanced the heat conductivity of current coolants such as water and ethylene glycol. Stated in [2], hybrid nanofluid is a new fluid created by distributing two different types of nanoparticles into the base fluid. According to experts, hybrid nanofluids, particularly those that work at very high temperatures, may eventually replace the conventional coolants. As a result, these nanofluids experience energy savings as well as less harmful effects on the environment [3]. Variety of nanofluids has been discovered through studies by researchers, for instance metal, metal nitrides/oxides/carbides, hybrid/composites and carbon. Literature survey has reported that significant attention was mostly directed to carbon-based nanofluids. Hence, the current endeavour focuses on copper and carbon nanotubes (CNTs) due to their excellent mechanical, electrical, and thermal properties. The addition of CNTs into a base fluid improves heat transfer performance significantly over metal-based nanofluids [4]. Several studies have been conducted on the performance of CNTs, both experimentally and numerically [5-7].

Hybrid nanofluids flow over a stretching sheet has captured many researchers attention [8]. Boundary layer flow passing through a stretching sheet has many applications in production and manufacturing processes, including wire drawing, polymer sheet, metal spinning, rubber sheet and polymer processing. These behaviours are crucial for solving engineering problems because the rate of cooling and the stretching process determine the necessary properties of the final product. Refer to [9], the heat generation/absorption effect on MHD bidirectional exponentially stretched sheet. It was revealed that the improved skin friction coefficient results from the impact of magnetic parameter and volume fraction of nanoparticles. According to [10], the axial flow profile of the hybrid nanofluid is reduced owing to rising volumetric concentration of hybrid nanomaterials. Recent investigation [11] on convectively heated stretched sheet disclosed that the larger values of the radiative parameter, Biot number and slip parameter significantly enhanced the ternary hybrid nanofluid's heat transfer rate.

Internal heat generation significantly affects the thermal performance of hybrid nanofluid. Authors in [12], addressed the effect of internal heat generation/absorption with hybrid nanofluid in an inclined porous cavity. Acccording to [13] the internal heat absorption with hall current and thermal radiation induced by stretched plate. The effect of heat

generation with chemically reactive bioconvective flow of hybrid nanofluid over curved stretchable surface. Was documented as stated in [14]. The impact of heat generation and thermal radiation was scrutinized stated in [15] from a wavy enclosure with entropy generation. The effect of aligned magnetic field on heat and flow have been studied by many scholars. Authors in [16], focused on the effect of aligned magnetic field over a stretched sheet in dusty Casson nanofluid. Focusing on similar surface, [17] considered the aligned magnetic field over an exponential stretching sheet with viscous dissipation and Newtonian heating. More recent studies on aligned magnetic field can be found in published articles by [18-21].

As disclosed by the above-mentioned literature survey, influence of aligned magnetic field and internal heat generation/absorption on carbon nanotube hybrid nanofluid from a stretched sheet has never been carried out. Therefore, the present study focuses on the stagnation point flow of carbon nanotube hybrid nanofluid past a stretching sheet with heat generation/absorption and aligned magnetic field. The Newtonian heating condition is accounted. Then, the partial differential equations (PDEs) are transformed to ordinary differential equations (ODEs) by using similarity transformation variables. The Runge-Kutta Fehlberg method (RKF45) is used to solve the resulting ODEs in Maple software.

2. METHODOLOGY

Two-dimensional steady flow on a stagnation point across a stretching sheet immersed in an incompressible viscous fluid of ambient temperature, T_∞. The stretching velocity $u_w(x)$ and the free stream velocity $u_\infty(x)$ are assumed to have the forms $u_w(x) = ax$ and $u_\infty(x) = bx$ respectively, where a and b are constants. The study [22] is extended by incorporating the effect of aligned angle parameter [23]. The governing equations involved are as follows:

$$u\frac{\partial u}{\partial x} + v\frac{\partial u}{\partial y} = 0, \tag{1}$$

$$u\frac{\partial u}{\partial x} + v\frac{\partial u}{\partial y} = U_\infty \frac{dU_\infty}{dx} + v_{hnf}\frac{\partial^2}{\partial y^2} - \frac{\sigma}{\rho}uB_0^2 sin^2\alpha_1, \tag{2}$$

$$u\frac{\partial T}{\partial x} + v\frac{\partial T}{\partial y} = \frac{k_{hnf}}{(\rho C_p)_{hnf}}\frac{\partial^2}{\partial y^2} + \frac{Q_0}{(\rho C_p)_{hnf}}(T - T_\infty), \tag{3}$$

subject to boundary conditions

$$u = u_w, v = 0, \frac{\partial T}{\partial y} = -h_sT, \text{ at } y = 0, \tag{4}$$

$$u \to U_\infty, T \to T_\infty, \text{ as } y \to \infty$$

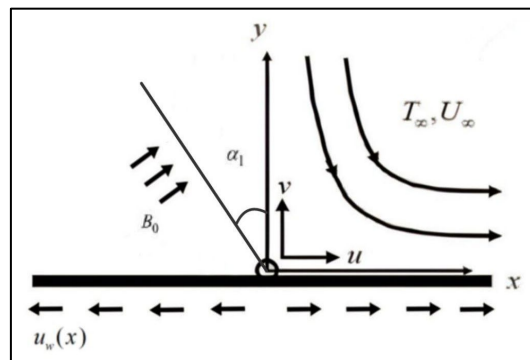where u and v are the velocity components along the x and y directions.

Figure 1. Coordinate system and physical model

The kinematic viscosity, dynamic viscosity, density, and thermal conductivity of a hybrid nanofluid are indicated by the letters v_{hnf}, μ_{hnf}, ρ_{hnf}, and k_{hnf}, accordingly. Further, T is the temperature inside the boundary layer, h_s is the heat transfer coefficient, σ is the electrical conductivity, $(\rho C_p)_{hnf}$ is the hybrid nanofluid's heat capacity and Q_0 is the dimensional heat generation or absorption coefficient. They can be expressed in terms of the properties of base fluid $_f$

and nanoparticles $_{s1,s2}$ as follows [22]:

$$v_{hnf} = \frac{\mu_{hnf}}{\rho_{hnf}}, \rho_{hnf} = (1-\phi_2)\left[(1-\phi_1)\rho_f + \phi_1\rho_{s1}\right] + \phi_2\rho_{s2}, \; \mu_{hnf} = \frac{\mu_f}{(1-\phi_1)^{2.5}(1-\phi_2)^{2.5}},$$

$$(\rho C_p)_{hnf} = (1-\phi_2)\left[(1-\phi_1)(\rho C_p)_f + \phi_1(\rho C_p)_{s1}\right] + \phi_2(\rho C_p)_{s2}, \tag{5}$$

$$\frac{k_{hnf}}{k_{bf}} = \frac{k_{s2} + 2k_{bf} - 2\phi_2(k_{bf} - k_{s2})}{k_{s2} + 2k_{bf} + \phi_2(k_{bf} - k_{s2})}, \frac{k_{bf}}{k_f} = \frac{k_{s1} + 2k_f - 2\phi_1(k_f - k_{s1})}{k_{s1} + 2k_f + \phi_1(k_f - k_{s1})}.$$

where ϕ_1 and ϕ_2 are the volume fractions of nanoparticles for *SWCNT* and *Cu* respectively. k_{hnf}, k_{bf}, k_{s1} and k_{s2} are the thermal conductivity of the hybrid nanofluid, base fluid, water, *SWCNT* and *Cu*. The solid nanoparticles of *Cu* ($\phi_2 = 0.1$) are added and mixed with a water-based liquid, then the solid nanoparticle of *SWCNT* ($\phi_1 = 0.06$) is added to the *Cu/water* nanofluid to create *SWCNT-Cu/water* hybrid nanofluid. The equations (1), (2) and (3) are nonlinear partial differential equations (PDEs) with many dependent variables which difficult to be solved directly. As a result, the governing PDEs is converted into ODEs using the similarity transformation variables as below:

$$\eta = \left(\frac{b}{v_f}\right)^{\frac{1}{2}} y, \quad \psi = (bv_f)^{\frac{1}{2}} x f(\eta), \quad \theta(\eta) = \frac{T - T_\infty}{T_\infty} \tag{6}$$

Equation (6) are the similarity transformation variables, where η, ψ and θ are non-dimensional similarity variables, stream function and temperature. The continuity equation (1) has satisfied by using Equation (6). Furthermore,

$$u = \frac{\partial \psi}{\partial y}, \quad v = -\frac{\partial \psi}{\partial x} \tag{7}$$

The ordinary differential equation can be acquired by substituting equation in (6) and (7) into the governing equations (2) and (3). Thus, the ODEs are as follows:

$$\frac{1}{(1-\phi_1)^{2.5}(1-\phi_2)^{2.5}\left[(1-\phi_2)\left[(1-\phi_1) + \phi_1\left(\frac{\rho_{s1}}{\rho_f}\right)\right] + \phi_2\left(\frac{\rho_{s2}}{\rho_f}\right)\right]} f''' + ff'' - f'^2 + 1 - Mf'\sin^2\alpha_1 = 0 \tag{8}$$

$$\frac{\frac{k_{hnf}}{k_f}\theta'' + \Pr\lambda\,\theta}{\left[(1-\phi_2)\left[(1-\phi_1) + \phi_1\frac{(\rho C_p)_{s1}}{(\rho C_p)_f}\right] + \phi_2\frac{(\rho C_p)_{s2}}{(\rho C_p)_f}\right]} + \Pr f\theta' = 0 \tag{9}$$

where $M = \frac{\sigma B_0^2}{\rho b}$ is the magnetic field parameter, $\gamma = h_s\left(\frac{v_f}{b}\right)^{1/2}$ is the conjugate parameter for Newtonian heating. $\lambda = \frac{Q_0}{b\rho C_p}$ is the heat source/sink parameter, $\varepsilon = \frac{a}{b}, (\varepsilon > 0)$ is the stretching parameter and $\Pr = \frac{v_f(\rho C_p)_f}{k_f}$ is the Prandtl number, where the value always constant at 6.2 for water-based fluid. The reduced boundary conditions are as follows:

$$f(0) = 0, \; f'(u_w) = \varepsilon, \; \theta'(0) = -\gamma(1 + \theta(0)), \tag{10}$$

$$f'(\eta) \to 1, \; f(\theta) \to 0, \; \theta(\eta) \to 0, \; as \; y \to \infty$$

The heat transfer rate $-\theta(0)$, the surface temperature $\theta(0)$, the skin friction coefficient $C_f = \frac{\tau_w}{\rho_f U^2_\infty}$ and the Nusselt number $Nu_x = \frac{xq_w}{k_f(T-T_\infty)}$ are the physical quantities of interest. The surface shear stress is $\tau_w = \mu_{hnf}\left(\frac{\partial u}{\partial y}\right)_{y=0}$. Thus, the $C_f Re_x^{1/2}$ and $Nu_x Re_x^{-1/2}$ are as below:

$$C_f Re_x^{1/2} = \frac{f''(0)}{(1-\phi_1)^{2.5}(1-\phi_2)^{2.5}}, \tag{11}$$

$$Nu_x Re_x^{-1/2} = -\frac{k_{hnf}}{k_f}\theta'(0), \tag{12}$$

where Reynolds number is indicated by $Re_x = \frac{U_\infty x}{v_f}$.

3. NUMERICAL METHODS

The resulting ordinary differential equations (8) and (9) with reduced boundary conditions (10) were solved numerically by using the RKF45 method. RKF45 is a numerical method that incorporates adaptive step size control and can be utilised to solve ODEs. Erwin Fehlberg, a renowned mathematician, first presented this numerical technique in 1969. The procedure for this method involves determining if the proper step size h is being employed. At each step, two distinct approximations for the solution are generated and compared. The approximation is accepted if the two outcomes are in close agreement. If the two outcomes do not agree on the required precision, the step size is decreased. If the solutions agree on more significant digits than necessary, the step size is raised. The following is the method for RKF45 of orders four and five [24]:

RKF of order four:

$$y_1 = y_0 + \frac{25}{216}k_1 + \frac{1408}{2565}k_3 + \frac{2197}{4104}k_4 + \frac{1}{5}k_5,$$

RKF of order five:

$$y_1 = y_0 + \frac{16}{135}k_1 + \frac{6656}{12825}k_3 + \frac{28561}{56430}k_4 - \frac{9}{50}k_5 + \frac{2}{55}k_6,$$

where:

$$k_1 = hf(x_0, y_0), \quad k_2 = hf\left(x_0 + \frac{h}{2}, y_0 + \frac{k_1}{2}\right),$$

$$k_3 = hf\left(x_0 + \frac{3h}{8}, y_0 + \frac{3k_1}{2} + \frac{9k_2}{32}\right),$$

$$k_4 = hf\left(x_0 + \frac{12h}{13}, y_0 + \frac{1932k_1}{2197} - \frac{7200k_2}{2197} + \frac{7296k_3}{2197}\right),$$

$$k_5 = hf\left(x_0 + h, y_0 + \frac{439k_1}{216} - 8k_2 + \frac{3680k_3}{513} - \frac{845k_4}{4104}\right),$$

$$k_6 = hf\left(x_0 + \frac{h}{2}, y_0 - \frac{8k_1}{27} + 2k_2 - \frac{3544k_3}{2565} + \frac{1859k_4}{4104} - \frac{11k_5}{40}\right).$$

To implement this method in the Maple software, an appropriate command, 'dsolve' is used with the option 'numeric'. Since this method combines the efficacy of the fourth-order and fifth-order Runge-Kutta methods, it provides exceptional reliability in solving ODEs [25]. As a result, the accuracy is improved.

4. RESULTS AND DISCUSSION

The numerical analysis is presented graphically on the velocity $f'(\eta)$ and temperature profiles $\theta'(\eta)$ to investigate various parameters which are stretching parameter ε, conjugate parameter γ, nanoparticle volume fractions for $SWCNT$ ϕ_1 and Cu ϕ_2, heat source/sink parameter λ, Prandtl number Pr, magnetic parameter M and aligned angle parameter α_1. Table 1 shows the values of thermophysical properties characteristic of water and nanoparticles used in this study [22].

Table 1. Thermophysical properties of water and nanoparticles

Physical Properties	Water (f)	SWCNT (ϕ_1)	Cu (ϕ_2)
$\rho \left(\frac{kg}{m^3} \right)$	997	2600	8953
$C_p \left(\frac{J}{kg \cdot K} \right)$	4179	425	385
$k \left(\frac{W}{m \cdot K} \right)$	0.613	6600	400

Comparison between the present results and prior numerical results have been carried out to validate the method's effectiveness as presented in Table 2. The obtained results for skin friction coefficient, $C_f Re^{1/2}{}_x$ values are compared with the studies from [22, 26-28]. Based on the comparison, it can be confirmed that the present result is verified as it came to a good agreement and great consistency. Thus, it is confirmed that the RKF45 method has proved its effectiveness and that the results of this study are regarded as precise and credible.

Table 2. The comparison of $C_f Re^{1/2}{}_x$ values for specific values of ε and $\phi_1 (Al_2O_3)$ with previous studies as $Pr = 6.2, \lambda = \phi_2 = 0$ and $\gamma = 1$

ε	ϕ_1	$C_f Re^{1/2}{}_x$

ε	ϕ_1	Bachok [26]	Yacob [27]	Mohamed [28]	Zaki [22]	Present
0.0	0.1	1.6019	1.6019	1.602081	1.602081384	1.602081414
	0.2	2.0584	2.0584	2.058376	2.058376034	2.058376152
0.5	0.1	0.9271	-	0.927121	0.927120763	0.927119925
	0.2	1.1912	-	1.191179	1.191176331	1.191176350
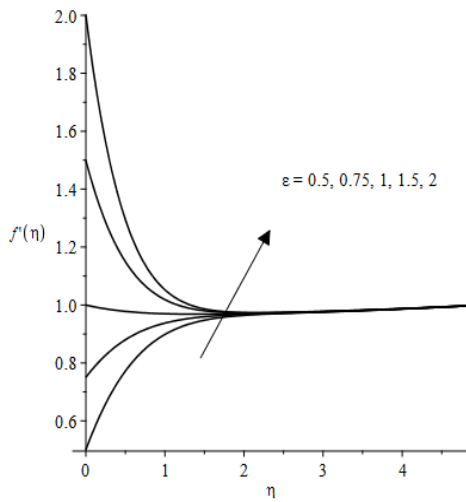
Figure 2. Velocity profiles $f'(\eta)$ for various ε when $Pr = 6.2, \ \lambda = 0.1, \ \gamma = 1, \ M = 0.3, \ \alpha_1 = \frac{\pi}{6}$
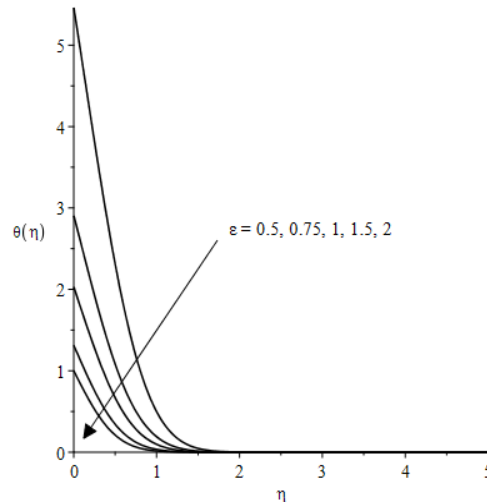

Figure 3. Temperature profiles $\theta(\eta)$ for various ε when $Pr = 6.2, \ \lambda = 0.1, \ \gamma = 1, \ M = 0.3, \ \alpha_1 = \frac{\pi}{6}$
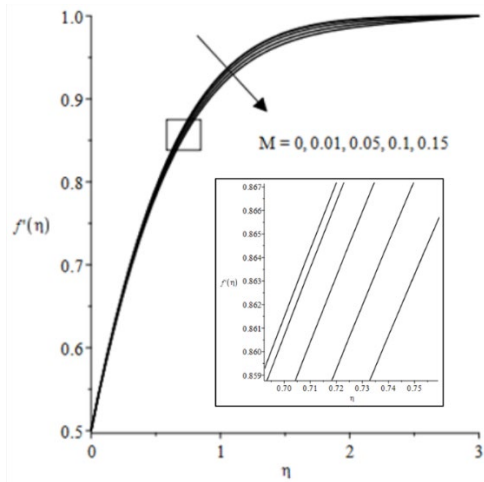
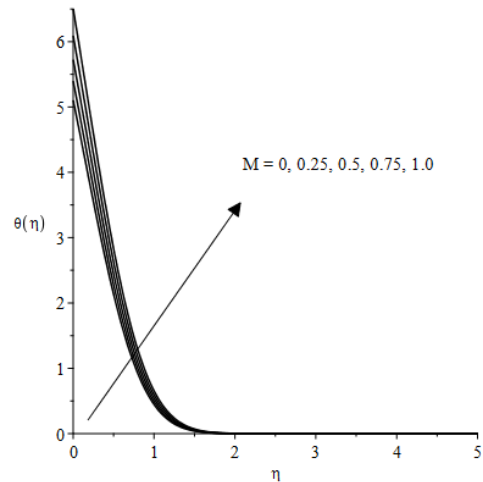**Figure 4.** Velocity profiles f'(η) for various M when $\varepsilon = 0.5, Pr = 6.2, \lambda = 0.1, \gamma = 1$

Figure 5. Temperature profiles θ(η) for various M when $\varepsilon = 0.5, Pr = 6.2, \lambda = 0.1, \gamma = 1$

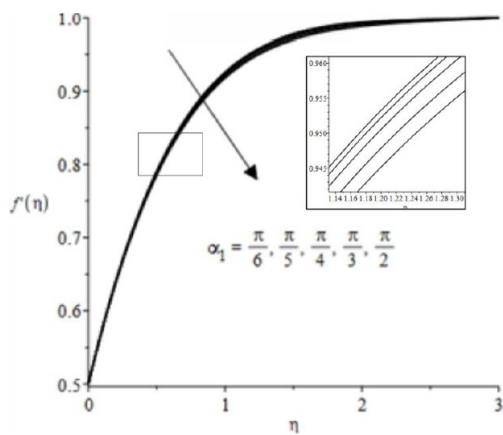

Figure 6. Velocity profiles f'(η) for various α_1 when $Pr = 6.2, \varepsilon = 0.5, \gamma = 1, M = 0.03, \lambda = 0.1$
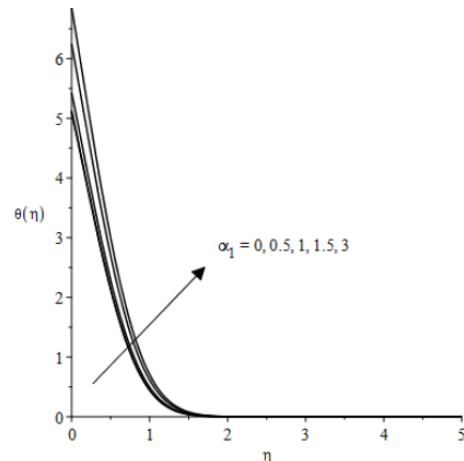

Figure 7. Temperature profiles θ(η) for various α_1 when $Pr = 6.2, \varepsilon = 0.5, \gamma = 1, M = 0.3, \lambda = 0.1$
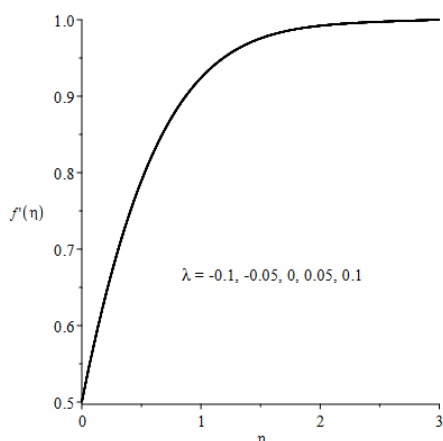

Figure 8. Velocity profiles f'(η) for various λ when $Pr = 6.2, \varepsilon = 0.5, \gamma = 1, M = 0.05, \alpha_1 = \frac{\pi}{6}$
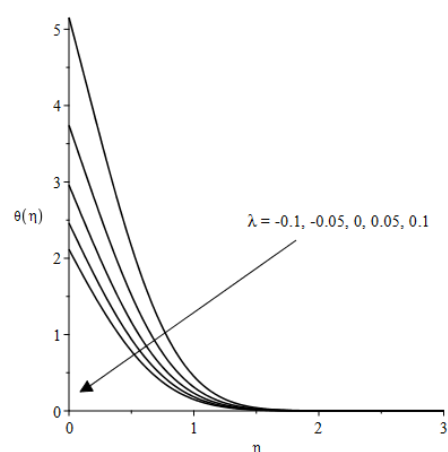

Figure 9. Temperature profiles θ(η) for various λ when $Pr = 6.2, \varepsilon = 0.5, \gamma = 1, M = 0.05, \alpha_1 = \frac{\pi}{6}$

Figures 2 and 3 show the graph of velocity and temperature profiles for the increasing value of stretching parameter ε when $Pr = 6.2, \lambda = 0.1, \gamma = 1, M = 0.3, \alpha_1 = \frac{\pi}{6}$. Based on figure 2, the velocity profile $f'(\eta)$ increases when ε

increases. The thickness of the boundary layer will increase due to increasing ε. Next, figure 3 shows the graph of the temperature profile $\theta(\eta)$ decreases with increasing ε. This is because the fluid is more likely to quickly exit the stagnation region when the stretching to external velocity ratio increases. In accordance with this situation, the sheet's surface temperature is dropped [22].

Figures 4 and 5 show the graph of velocity and temperature profiles for the increasing magnetic field parameter M when $\varepsilon = 0.5, Pr = 6.2, \lambda = 0.1, \gamma = 1$. The presence of magnetic field tends to influence the fluid movement because it creates a force known as the Lorentz force that works against the flow. Consequently, this causes the velocity profile to decline. The velocity profile in figure 4 is decreased because of the fluid flow slows down by the imposed magnetic field [29]. Figure 5 shows the graph of the temperature profile $\theta(\eta)$ increases with increasing M. In a flowing fluid, the magnetic field may cause the Lorentz force, a drag force that slows the flow and increases the temperature.

Figures 6 and 7 show the graph of the velocity and temperature profile for the increasing aligned angle α_1 when $Pr = 6.2, \varepsilon = 0.5, \gamma = 1, \lambda = 0.1, M = 0.03$ and $M = 0.3$. The increment value of aligned angle α_1 results in decreasing velocity and increasing temperature profiles. This statement is supported by [11], which stated that the increasing value of aligned angle increases the strength of magnetic field, which act in opposite direction of the flow region. This enhances the Lorentz force that decelerates fluid flow and increases the temperature.

Figures 8 and 9 show the graph of velocity and temperature profiles for increasing heat source/sink parameter λ when $Pr = 6.2, \varepsilon = 0.5, \gamma = 1, M = 0.05, \alpha_1 = \frac{\pi}{6}$. The increasing λ in figure 8 does not affect the velocity profile as the equation is not linked to each other due to decouple boundary layer equation. This indicates that the λ is not present in the momentum equation. Figure 9 shows the graph of the temperature profile $\theta(\eta)$ decreases with increasing λ. The presence of heat absorption ($\lambda < 0$) causes the temperature profile and its boundary layer thickness to reduce since heat is removed from the plate. Studies from [30], supports the above results even more, where they discovered that lowering the surface temperature causes the heat absorption/generation coefficient to rise, thus reducing the conductive thermal resistance.

5. CONCLUSIONS

The numerical solutions for different parameters of stretching parameter ε, heat source/sink parameter λ, magnetic parameter M and aligned angle parameter α_1 towards the velocity $f'(\eta)$ and temperature profiles $\theta(\eta)$ are solved by utilising RKF45 method. The results have shown how the stretching parameter ε, heat source/sink parameter λ, magnetic parameter M and aligned angle α_1 affect the flow of fluid and heat transfer characteristics. The results of this study are important for industrial practitioners who works in industries like energy, aerospace, automotive, oil and gas and many more.

DECLARATION OF ORIGINALITY

The authors declare no conflict of interest to report regarding this study conducted.

REFERENCES

[1] Mehmood T, Ramzan M, Howari F, Kadry S, Chu Y. Application of response surface methodology on the nanofluid flow over a rotating disk with autocatalytic chemical reaction and entropy generation optimization. Scientific Reports. 2021;11(1):4021.

[2] Jamil F, Ali HM. Applications of hybrid nanofluids in different fields. In Hybrid nanofluids for convection heat transfer 2020 Jan 1 (pp. 215-254). Academic Press.

[3] Yang L, Ji W, Mao M, Huang J. An updated review on the properties, fabrication and application of hybrid-nanofluids along with their environmental effects. Journal of Cleaner Production. 2020;257:120408.

[4] Habib NA, Arifin NS, Zokri SM, Kasim AR. MHD flow of dusty Jeffrey fluid flow containing carbon nano tubes (CNTs) under Influences of Viscous Dissipation and Newtonian heating. Malaysian Journal of Mathematical Sciences. 2024 Jun 1;18(2).

[5] Scott TO, Ewim DR, Eloka-Eboka AC. Experimental investigation of natural convection Al_2O_3-MWCNT/water hybrid nanofluids inside a square cavity. Experimental Heat Transfer. 2024;37(3):294-312.

[6]   Alfellag MA, Kamar HM, Abidin U, Kazi S, Sidik NAC, Muhsan AS, Alawi OA. Optimizing mixing ratio of multi-walled carbon nanotubes and titanium dioxide: A green approach to high-performance hybrid nanofluids for heat transfer. Powder Technology. 2024;436:119509.

[7]   Majeed A, Amanat A, Mary GLR, Altohamy AA, Alsayegh R, Khan SU, Kolsi L, Sreelakshmi K. Thermally developed radiated flow of single and multiple carbon nanotubes (SWCNTs-MWCNTs) with variable thermal conductivity. Journal of Radiation Research and Applied Sciences. 2025;18(1):101244.

[8]   Hussain SM. Numerical assessment of a sutterby hybrid nanofluid over a stretching sheet with a particle shape factor. Waves in Random and Complex Media. 2023;1-17.

[9]   Zainal NA, Nazar R, Naganthran K, Pop I. Heat generation/absorption effect on MHD flow of hybrid nanofluid over bidirectional exponential stretching/shrinking sheet. Chinese Journal of Physics. 2021;69:118-33.

[10] Farooq U, Tahir M, Waqas H, Muhammad T, Alshehri A, Imran M. Investigation of 3D flow of magnetized hybrid nanofluid with heat source/sink over a stretching sheet. Scientific Reports. 2022;12(1):12254.

[11] Sharma RP, Badak K. Heat transport of radiative ternary hybrid nanofluid over a convective stretching sheet with induced magnetic field and heat source/sink. Journal of Thermal Analysis and Calorimetry. 2024;149(9):3877-89.

[12] Chamkha AJ, Armaghani T, Mansour MA, Rashad AM, Kargarsharifabad H. MHD convection of an Al_2O_3–Cu/water hybrid nanofluid in an inclined porous cavity with internal heat generation/absorption. Iranian Journal of Chemistry and Chemical Engineering. 2022;41(3):936-56.

[13] Kodi R, Ravuri MR, Veeranna V, Khan MI, Abdullaev S, Tamam N. Hall current and thermal radiation effects of 3D rotating hybrid nanofluid reactive flow via stretched plate with internal heat absorption. Results in Physics. 2023;53:106915.

[14] Haq F, Ur Rahman M, Gupta M. Theoretical assessment of chemically reactive bioconvective flow of hybrid nanofluid by a curved stretchable surface with heat generation. International Journal of Modelling and Simulation. 2024 Aug 25:1-2.

[15] Hussain SM, Parveen R, Katbar NM, Rehman S, Abd-Elmonem A, Abdalla NSE, Ahmad H, Qureshi MA, Jamshed W, Amjad A. Entropy generation analysis of MHD convection flow of hybrid nanofluid in a wavy enclosure with heat generation and thermal radiation. Reviews on Advanced Materials Science. 2024;63(1):20240037.

[16] Arifin NS, Kasim ARM, Zokri SM, Haryatie SF, Salleh MZ. Dusty Casson fluid flow containing single-wall carbon nanotubes with aligned magnetic field effect over a stretching sheet. CFD Letters. 2023;15(1):17-25.

[17] Habib NANN, Arifin NS, Zokri SM, Kasim ARM. Aligned MHD Jeffrey fluid flow containing carbon nanoparticles over exponential stretching sheet with viscous dissipation and Newtonian heating effects. Journal of Advanced Research in Fluid Mechanics and Thermal Sciences. 2023;106(1):104-15.

[18] Ramana RM, Maheswari C, Shaw SM, Dharmaiah G, Fernandez-Gamiz U, Noeiaghdam S. Numerical investigation of 3-D rotating hybrid nanofluid Forchheimer flow with radiation absorption over a stretching sheet. Results in Engineering. 2024;22:102019.

[19] Norani AA, Jiann LY, Kamal MHA, Shafie S, Rawi NA. The effects of an aligned magnetic field on nanofluid flow with Newtonian heating. CFD Letters. 2024;16(4):111-9.

[20] Rath C, Nayak A. MHD second-grade nanofluid slip flow over a stretching sheet subject to activation energy, thermophoresis, and Brownian effects. Physica Scripta. 2024;99(3):035228.

[21] Pal D. Impact of Arrhenius activation energy on thin film flow in nonlinearly thermally radiative kerosene-based ferro-nanofluid with aligned magnetic field. International Journal of Ambient Energy. 2025;46(1):2446513.

[22] Zaki AMM, Mohammad NF, Soid SK, Mohamed MKA, Jusoh R. Effects of heat generation/absorption on a stagnation point flow past a stretching sheet carbon nanotube water-based hybrid nanofluid with Newtonian heating. Malaysian Journal of Applied Sciences. 2021;6(2):34-47.

[23] Kasim AR, Arifin NS, Zokri SM, Salleh MZ. Flow and heat transfer of aligned magnetic field with Newtonian heating boundary condition. In MATEC Web of Conferences 2018 (Vol. 189, p. 01005). EDP Sciences.

[24] Arora G, Joshi V, Garki IS. Developments in Runge–Kutta method to solve ordinary differential equations. Recent Advances in Mathematics for Engineering. 2020;193-202.

[25] Zhang L. Studying and Comparing Numerical Methods for Ordinary Differential Equations. 2015.

[26] Bachok N, Ishak A, Pop I. Stagnation-point flow over a stretching/shrinking sheet in a nanofluid. Nanoscale Research Letters. 2011;6:1-10.

[27] Yacob NA, Ishak A, Pop I. Falkner–Skan problem for a static or moving wedge in nanofluids. International Journal of Thermal Sciences. 2011;50(2):133-9.

[28] Mohamed MK, Ong HR, Alkasasbeh HT, Salleh MZ. Heat transfer of ag-Al2O3/water hybrid nanofluid on a stagnation point flow over a stretching sheet with Newtonian heating. In Journal of Physics: Conference Series 2020 Apr 1 (Vol. 1529, No. 4, p. 042085). IOP Publishing.

[29] Gurrampati VRR. Cattaneo-Christov heat and mass transfer flux across electro-hydrodynamics blood-based hybrid nanofluid subject to Lorentz force. CFD Letters. 2022;14(7):124-34.

[30] Bhattacharya P, Samanta AN, Chakraborty S. Numerical study of conjugate heat transfer in rectangular microchannel heat sink with Al_2O_3/H_2O nanofluid. Heat and Mass Transfer. 2009;45:1323-33.